

# ARVCF Depletion Cooperates with Tbx1 Deficiency in the Development of 22q11.2DS-like Phenotypes in *Xenopus*

Hong Thi Tran,<sup>1,2†</sup> Mieke Delvaeye,<sup>1,2†</sup> Veerle Verschuere,<sup>1,2</sup> Emilie Descamps,<sup>3</sup> Ellen Crabbe,<sup>1,2</sup> Luc Van Hoorebeke,<sup>4</sup> Pierre McCrea,<sup>5</sup> Dominique Adriaens,<sup>3</sup> Frans Van Roy,<sup>1,2</sup> and Kris Vleminckx<sup>1,2\*</sup>

The 22q11.2 deletion syndrome is a common dominant genetic disorder characterized by a heterozygous deletion of a cluster of genes on chromosome 22q11.2. *TBX1*, a transcription factor belonging to the T-box gene family, is a key player in the syndrome. However, heterozygosity of *Tbx1* in mouse models does not fully recapitulate the phenotypes characteristic of the disease, which may point to the involvement of other genes in the deleted chromosomal region. Hence, we investigated the contribution of the catenin *ARVCF*, another gene that is deleted in 22q11.2DS. During *Xenopus* development, *ARVCF* mRNA is expressed in the pharyngeal arches and depleting either *ARVCF* or *Tbx1* results in delayed migration of the cranial neural crest cells and in defects in the craniofacial skeleton and aortic arches. Moreover, double depletion of *ARVCF* and *Tbx1* revealed that they act cooperatively, indicating that decreased *ARVCF* levels may also contribute to 22q11.2DS-associated phenotypes. *Developmental Dynamics* 240:2680–2687, 2011. © 2011 Wiley Periodicals, Inc.

**Key words:** *Xenopus*; ARVCF; TBX1; DiGeorge; velo-cardio-facial syndrome; p120 catenin

Accepted 21 September 2011

## INTRODUCTION

Humans with DiGeorge syndrome (DGS) usually have a monoallelic deletion of 3 Mbp in chromosome

22q11.2. The deletions and symptoms of DGS are similar to those of the velo-cardio-facial syndrome (VCFS) and the conotruncal anomaly face syndrome (CAFS). These three

syndromes are collectively known as the 22q11 deletion syndrome (22q11.2DS), which is associated with congenital heart defects, malformation of facial bones, thymic

**ABBREVIATIONS** CNCC cranial neural crest cells CT computed tomography DGS DiGeorge syndrome MO morpholino NCC neural crest cell VCFS velocardiocardial syndrome

Additional Supporting Information may be found in the online version of this article.

<sup>1</sup>Department for Molecular Biomedical Research, VIB, Ghent, Belgium

<sup>2</sup>Department of Biomedical Molecular Biology, Ghent University, Ghent, Belgium

<sup>3</sup>Evolutionary Morphology of Vertebrates, Ghent University, Ghent, Belgium

<sup>4</sup>UGCT, Department of Physics and Astronomy, Ghent University, Ghent, Belgium

<sup>5</sup>Department of Biochemistry and Molecular Biology, Program in Genes and Development, University of Texas M.D. Anderson Cancer Center, Houston, Texas

Grant sponsor: Research Foundation-Flanders (FWO); Belgian Federation against Cancer; "Geconcerteerde Onderzoeksacties of Ghent University."

<sup>†</sup>H.T. Tran and M. Delvaeye contributed equally to this work.

\*Correspondence to: Kris Vleminckx, Ph.D., Department for Molecular Biomedical Research, VIB & Ghent University, 9052 Ghent, Belgium. E-mail: kris.vleminckx@dmbr.UGent.be

DOI 10.1002/dvdy.22765

Published online 25 October 2011 in Wiley Online Library (wileyonlinelibrary.com).

hypoplasia, velopharyngeal dysfunction, hypocalcemia, learning and psychiatric disorders. Most of the structures affected are derivatives of the pharyngeal arches, which consist of different cell populations: the ectoderm, the endoderm, the mesoderm, and the neural crest cells (NCC) (reviewed in Yamagishi and Srivastava, 2003; Baldini, 2005).

Many studies have demonstrated that *TBX1* is the key player in the development of 22q11.2DS. *TBX1* encodes a transcription factor belonging to a protein family characterized by a strongly conserved DNA-binding domain, the T-box. These transcription factors can function either as activators or repressors (reviewed in Wilson and Conlon, 2002). Support for a central role of the *TBX1* gene in human 22q11.2DS is emerging (Yagi et al., 2003; Stoller and Epstein, 2005). Moreover, heterozygous knockout of *Tbx1* in mice phenocopies the cardiovascular defects observed in 22q11.2DS patients, although it does not generate the full spectrum of the disorder (Jerome and Papaioannou, 2001; Lindsay, 2001; Merscher et al., 2001). Experimental analyses in the mouse and association studies in humans have indicated that deficiencies in *TBX1* and *GNBL1*, another gene deleted in 22q11.2DS, may underlie the psychiatric aspects associated with the syndrome (Paylor et al., 2006). In addition, the variable manifestation of congenital heart defects in 22q11.2DS patients could be the result of mutations in the remaining *TBX1* allele (Rauch et al., 2004). Zebrafish *van gogh* (*vgo*) mutants, which contain a nonsense mutation in the *Tbx1* gene, have defects in the inner ear and the pharyngeal arches, and in associated structures such as the thymus (Piotrowski et al., 2003). In *Xenopus*, expression of a dominant-negative variant of *Tbx1*, as well as its morpholino-mediated *Tbx1* depletion, leads to defects in the cranial cartilage and the head muscles (Ataliotis et al., 2005; Tazumi et al., 2010).

Another gene that is also deleted in 22q11.2DS is *ARVCF* (armadillo repeat gene deleted in VCFS), encoding a member of the p120 catenin fam-

ily, which is involved in cell–cell adhesion (reviewed in Hatzfeld, 2005). *ARVCF* binds to the cytoplasmic domain of classical cadherins and is involved in the regulation of their stability (Davis et al., 2003). Depletion of *ARVCF* in *Xenopus* leads to defects in gastrulation and axial elongation, probably due to its involvement in regulation of Rho GTPase activity (Fang et al., 2004). It appears that reduction of *ARVCF* levels in mice is by itself insufficient to cause the phenotypes associated with 22q11.2DS, because a heterozygous deletion of a region of 16 genes, including *Arvcf*, does not result in cardiovascular defects (Puech et al., 2000). Evidently, this does not exclude the possibility that heterozygosity of *ARVCF* contributes to the phenotypes associated with reduced expression levels of other genes deleted in 22q11.2DS.

In this study, we show that *ARVCF* is expressed during different stages of development in *Xenopus laevis*, and that transcripts are enriched in specific structures and tissues, such as the pharyngeal arches and the otic vesicle. To investigate the potential role of *ARVCF* and *Tbx1* deficiency with relation to phenotypes associated with 22q11.2DS during development of *X. laevis*, we depleted both proteins using morpholinos. Our data point to the involvement of both *ARVCF* and *Tbx1* in the development of 22q11.2DS-like phenotypes and show the utility of using *X. laevis* as a model system for studying this syndrome.

## RESULTS

### Expression Pattern of *ARVCF* During the Development of *X. laevis*

It has been demonstrated by RT-PCR that *ARVCF* is expressed during different stages of development and in several tissues of adult *X. laevis* (Paulson et al., 2000). However, its exact spatiotemporal expression pattern during development has not been documented. Here, we analyzed *ARVCF* mRNA expression from gastrula until early tadpole stage by whole-mount in situ hybridization (Fig. 1). During gastrulation, *ARVCF* mRNA is located in the spreading ectoderm (data not shown), and it is

further expressed in all ectodermal derivatives. At neurulation, it is enriched in the neural plate region and the bordering neural crest (Fig. 1a). In late tailbuds (stage 26) and early tadpoles (stage 31), *ARVCF* is present throughout the epidermis and is concentrated in distinct regions associated with morphogenetic movements, i.e., optic vesicle, ear vesicle, olfactory placode, heart anlage, pharyngeal arches (including the cranial neural crest), and brain (Fig. 1b,e). The migrating cranial neural crest cells in stage-26 embryos are clearly enriched in *ARVCF* transcripts (Fig. 1c,d).

### Knockdown of *ARVCF* Results in Malformations of the Craniofacial Cartilage and Abnormalities in the Aortic Arches

The in situ hybridization expression pattern of *Xenopus ARVCF* and the fact that *ARVCF* is deleted in 22q11.2DS prompted us to investigate if this protein plays a role in the development of the structures affected in 22q11.2DS. To deplete *ARVCF*, a previously described morpholino directed against its 5' UTR (*ARVCF* MO, Fang et al., 2004) was injected in four- or eight-cell-stage embryos. As a control, a morpholino directed against an irrelevant sequence was used (control MO). For phenotypic analysis, embryos were injected with *ARVCF* MO or control MO in the dorsal blastomeres in the animal region in order to target the cranial and cardiac NCCs (Moody, 1987). Injection of 40 ng of the *ARVCF* MO caused 47% reduction in endogenous *ARVCF* levels (see Supp. Fig. S1, which is available online) and, when injected at the one-cell stage, led to gastrulation defects (data not shown and Fang et al., 2004). However, most embryos injected with a similar dose of *ARVCF* MO at the four- or eight-cell stage underwent normal gastrulation and initially developed normally. The resulting tadpoles were processed at stage 48 for immunostaining with an antibody directed against the von Willebrand factor (vWF) to observe the aortic arches. In normal development, only three of the six aortic arches remain at stage 48, namely arches 3, 4, and 5 (Levine et al., 2003). The development of these aortic arches was

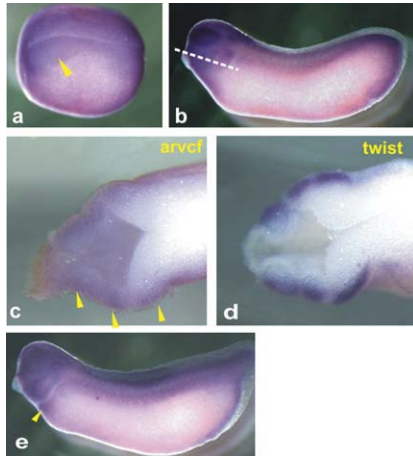


**Fig. 1.** Determination of the expression pattern of ARVCF by whole-mount in situ hybridization. *X. laevis* embryos at different developmental stages were examined using an antisense probe directed against ARVCF. **a:** Lateral view of stage-18 embryo with dorsal side at the top, anterior to the left. The arrow-head shows enriched transcripts in the neural plate and bordering neural crest. **b:** Lateral view of a stage-26 tailbud with the anterior towards the left. The line shows the position of the section shown in panel c. **c:** Horizontal section through the head region of a stage-26 tailbud showing the presence of ARVCF transcripts in the cranial neural crest cells (yellow arrowhead). **d:** A similar section of a stage-26 embryo stained with the neural crest marker *Twist* as a reference. **e:** Stage-31 early tadpole showing enriched ARVCF expression in the head region and the heart (yellow arrowhead).

severely affected in embryos injected with the ARVCF MO (Fig. 2A and Table 1), and aortic arch 5 was usually missing (Fig. 2A, d–f) or severely underdeveloped (data not shown). In addition, fewer bifurcations were observed on aortic arches 3 and 4. Importantly, these aortic arch defects could be rescued to a large extent by coinjecting 20 pg of ARVCF RNA lacking the morpholino-recognition sequence (Supp. Fig. S2 and Table 1).

Alcian Blue staining, which reveals the cartilage structures of the head, showed that all the facial structures, such as Meckel's cartilage, the ceratobranchials, and the ceratohyal cartilage, were present in embryos injected with the ARVCF MO (Fig. 2B,C). However, malformations of Meckel's and ceratohyal cartilage were observed in 42% of the embryos injected with ARVCF MO (Fig. 2B and Table 1) and heads were more narrow (Fig. 2C). These defects were substantially rescued by coinjection of ARVCF RNA

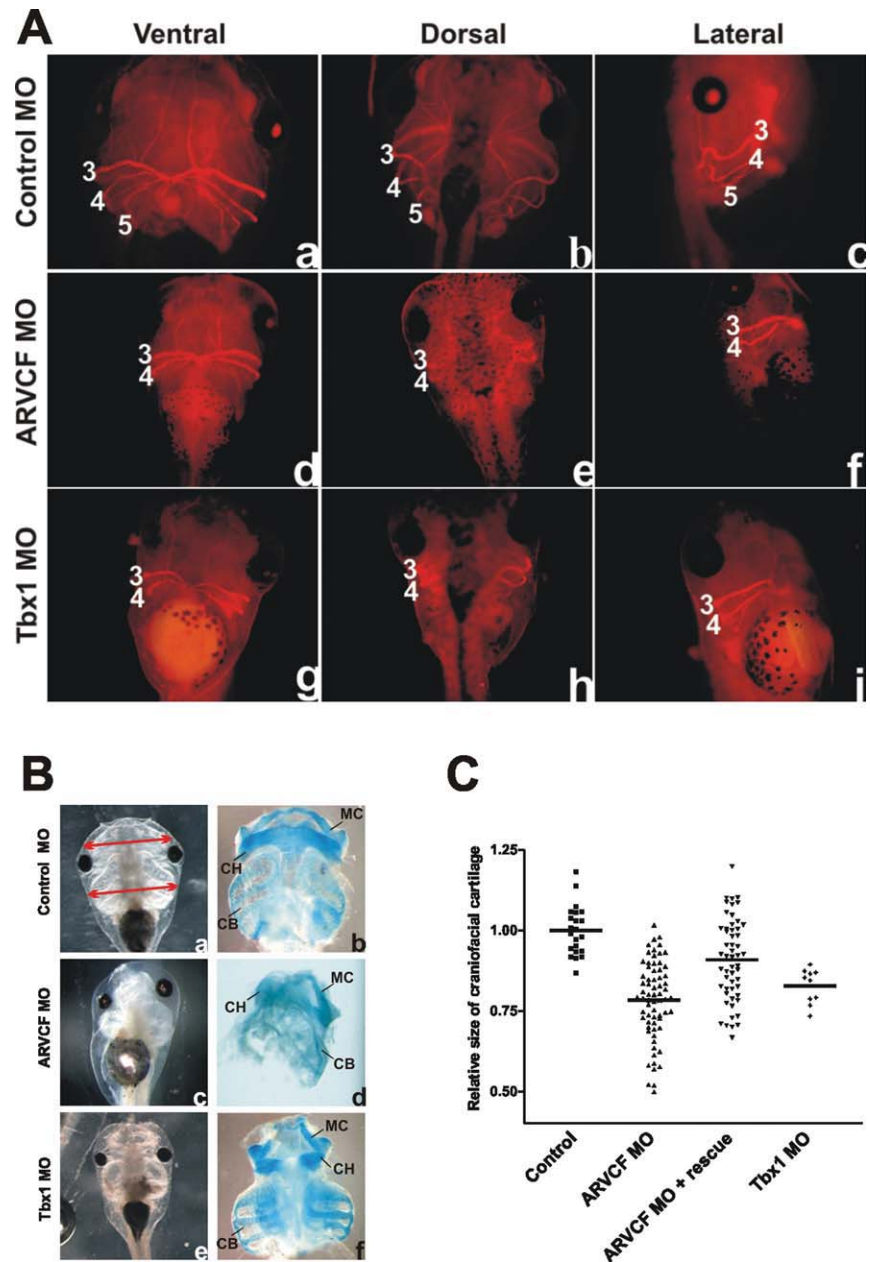


**Fig. 2.** Defects in the aortic arches and the craniofacial skeleton after depletion of ARVCF or Tbx1. **A:** To evaluate aortic arch formation, 50 ng of ARVCF MO or control MO was injected at the eight-cell stage (d–f), or 50 ng Tbx1 MO (g–i) or control MO (a–c) at the one-cell stage. To visualize the aortic arches, embryos were fixed at stage 48 and stained with the von Willebrand factor antibody. This antibody stains mainly the aortic arches (aa) connected to the heart (arches are numbered). At this stage, three pairs of aortic arches are normally present: arches 3, 4, and 5. Depletion of ARVCF frequently results in total loss of aortic arch 5 and less developed arches 3 and 4 (d–f). Knockdown of Tbx1 also results in defects in aortic arch development (g–i). Again, aortic arch 5 is often missing while the others are less developed. **B:** Embryos were injected at the four- or eight-cell stage in two dorsal blastomeres with 50 ng ARVCF MO (c,d), or at the one-cell stage with 50 ng Tbx1 MO (e,f) or control MO (a,b). Tadpoles were injected at stage 48 either alive (left) or fixed and stained with Alcian Blue to reveal the cartilage structures (right). Knockdown of ARVCF or Tbx1 results in malformation of the cartilage structures of the head. Meckel's cartilage (MC) and the ceratohyal cartilage (CH) are malformed. The ceratobranchial cartilage (CB) is also affected in tadpoles injected with ARVCF MO or Tbx1 MO. **C:** The heads of embryos injected with ARVCF MO or Tbx1 MO were significantly narrower than those of control embryos ( $P < 0.0001$ ), and this phenotype could be rescued by coinjection with 20 pg of ARVCF RNA that lacks the 5'UTR and can not be targeted by the morpholino ( $P < 0.0001$ ).



TABLE 1. Percentages of Aortic Arch Defects and Cartilage Malformations

Injection	Aortic arch defects (%) <sup>a</sup>	n	Malformation of cartilage (%) <sup>b</sup>	n
Control MO (50 ng)	0	74 (4)	2.5	91 (4)
ARVCF MO (50 ng)	69	80 (6)	42	113 (8)
ARVCF MO (50 ng) + 20 pg ARVCF RNA	26	50 (3)	21	48 (4)
TBX1 MO (50 ng)	63	111 (4)	51.5	79 (4)
ARVCF MO (20 ng)	4	22 (2)	3	55 (3)
TBX1 MO (20 ng)	0	24 (2)	2	76 (3)
TBX1 MO (20 ng) + ARVCF MO (20 ng)	29	35 (2)	30	51 (3)

<sup>a</sup>Aortic arch defects are defined by either fewer bifurcations or a missing aortic arch 5.  
<sup>b</sup>Malformation of the cartilage is defined as abnormalities in the shape of Meckel's cartilage and the ceratohyal cartilage.

g-i), and fewer bifurcations were observed on aortic arches 3 and 4 compared to the controls (Fig. 2A). Injection of 50 ng of Tbx1 MO also led to malformations of the cartilage structures of the head at stage 48 compared with embryos injected with control MO (Fig. 2B,C and Table 1). Meckel's cartilage and the ceratohyal cartilage were frequently malformed (Fig. 2B,C). Like the effects of ARVCF MO, a significant reduction in the width of the head was observed in tadpoles injected with Tbx1 MO (Fig. 2C). Both the defects in the aortic arches and the narrowing of the head could be rescued by the coinjection of a synthetic Tbx1 RNA that could not be recognized by the Tbx1 MO (Supp. Fig. S3).

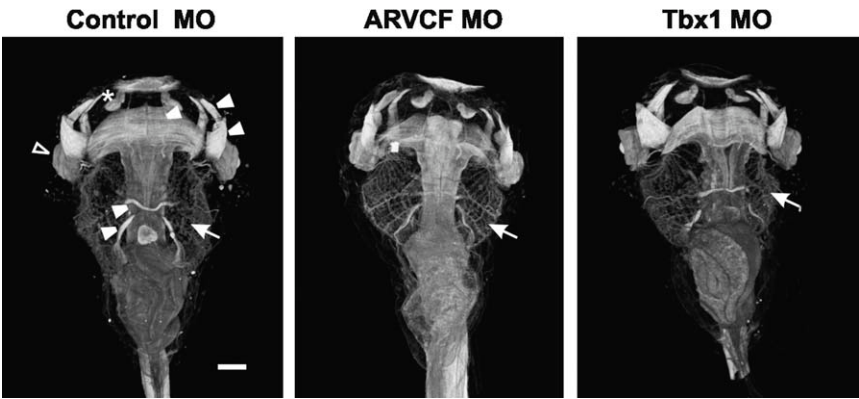


Fig. 3. Three-dimensional reconstructions of CT-scanning images of embryos injected with ARVCF or Tbx1 MO (scale bar = 0.25 mm). Embryos at the four-cell stage were injected in one dorsal blastomere with 40 ng of Control MO, ARVCF MO, or Tbx1 MO, together with a fluorescent tracer. Tadpoles were fixed at stage 48 and subjected to CT-scanning. All reconstructions are shown in ventral view. Structures visible are the eyes (open arrowhead), the olfactory placode and vomeronasal organ (asterisk), the cranial muscles (closed arrowheads), and the branchial basket (arrows). The 3D-reconstructions reveal that injection of ARVCF MO or Tbx1 MO results in the reduction of the gill apparatus (arrows).

(Fig. 2C and Table 1). Together, these results show that depletion of ARVCF in *Xenopus* embryos generates developmental malformations comparable to the defects observed in 22q11.2DS.

Knockdown of Tbx1 Results in Defects of the Facial Cartilage and Aortic Arches

Several studies have demonstrated that absence of *Tbx1* in mice and zebrafish generates phenotypes that resemble malformations observed in humans with 22q11.2DS (Jerome and Papaioannou, 2001; Lindsay, 2001; Merscher et al., 2001; Piotrowski

et al., 2003). We wanted to determine if morpholino-mediated depletion of *Tbx1* in *Xenopus* embryos results in similar defects. Hence, we designed a morpholino against a region encompassing the start codon to effectively deplete the *Tbx1* protein (Supp. Fig. S1). Embryos were injected with 50 ng of either *Tbx1* MO or control MO. At stage 48, embryos were stained with the vWF antibody to observe the aortic arches, and with Alcian Blue to reveal the cartilage structures (Fig. 2). Depletion of *Tbx1* generated defects in the aortic arches (Fig. 2A) similar to those seen after knockdown of ARVCF. Again, aortic arch 5 was underdeveloped and sometimes absent (Fig. 2A,

Gross Anatomical Evaluation of the Larval Head Region by Micro-CT Scanning

We also investigated whether the aortic arch abnormalities observed in tadpoles depleted of ARVCF or *Tbx1* could be secondary to gross general structural malformations in the head region. We injected embryos at the four-cell stage unilaterally with morpholino and a fluorescent tracer in one dorsal blastomere. Stage-48 tadpoles were fixed, stained with phosphotungstic acid, and scanned by micro-CT (Fig. 3). Several structures, including the brain, the cranial muscles, and the gill apparatus, could be observed in three dimensions. This examination confirmed that tadpoles injected with ARVCF or *Tbx1* MO had a smaller gill apparatus, the basis of which is the ceratobranchial cartilage. It also showed that all structures that are visible in control tadpoles, including the muscles and the branchial basket, were present and correctly patterned. These results make it unlikely that the aortic arches are non-specifically affected in ARVCF or *Tbx1* MO-injected embryos.

ARVCF and Tbx1 Depletion Delays Cranial Neural Crest Cell Migration

As described above, injection of either ARVCF or *Tbx1* MO led to malformations in the cartilage structures of the head (Fig. 2). Because these

structures are derived mainly from the cranial neural crest cells (CNCC), we wanted to find out if the specification and/or migration of these cells is disturbed by depletion of ARVCF or Tbx1. Embryos were injected unilaterally at the four-cell stage with ARVCF, Tbx1, or control MO, together with a tracer RNA. Neural crest specification and migration was then examined by in situ hybridization for the marker genes *Twist* (Fig. 4) and *Slug* (data not shown) at stage 20, when CNCC have initiated their migration, and at successive stages 27 and 32, when they have reached their final destination in the head. Knockdown of ARVCF or Tbx1 did not result in loss of CNCC, and their specification was apparently normal at stage 20 (Fig. 4). All three streams of migrating CNCC that can be revealed by the *Slug* or *Twist* probes were discernable, namely the mandibular, hyoid, and branchial streams. However, the migration of the CNCC in the different streams was delayed in embryos injected with ARVCF MO (57% affected,  $n = 36$ ) or Tbx1 MO (80% affected,  $n = 21$ ) compared to the non-injected side (Fig. 4), but it was not delayed in embryos injected with control MO. At stage 32, no differences between the injected and non-injected side could be observed for any of the injection setups (Fig. 4), indicating that the defect observed is indeed delayed migration and not a premature stop in migration. Together, our results show that depletion of neither ARVCF nor Tbx1 influences NCC specification. However, depletion of ARVCF or Tbx1 delays the migration of the CNCCs in the pharyngeal arches.

### Cooperative Effect of ARVCF and Tbx1 Depletion on the Development of the Cartilage and the Aortic Arches

Our data show that although ARVCF and Tbx1 may be active in different cell types, they both regulate the formation of craniofacial and cardiovascular structures. To look for potential cooperative activity, we depleted ARVCF and Tbx1 simultaneously. As ARVCF and Tbx1 morpholinos work in a dose-dependent way, we combined silent doses of both MOs and examined the

cartilage and aortic arch phenotypes. Injection of 20 ng of either Tbx1 MO or ARVCF MO did not lead to any noticeable phenotypic change in *Xenopus* embryos. In contrast, combined injection of 20 ng of each morpholino at the one-cell stage generated phenotypes similar to those observed with single injections of the effective dose (50 ng), namely defects in the cartilage structures of the head and in the aortic arches (Fig. 5 and Table 1). After depletion of both ARVCF and Tbx1, aortic arch 5 was usually missing, and, when present, it was severely underdeveloped, as were arches 3 and 4 (Fig. 5A, f). In addition, Meckel's and ceratohyal cartilage were malformed in embryos injected with both ARVCF MO and Tbx1 MO, but not in the different controls (Fig. 5A). Heads of embryos injected simultaneously with both morpholinos were significantly smaller than in controls (Fig. 5B). Also, migration of CNCC was markedly delayed in the embryos injected unilaterally with 20 ng ARVCF MO in combination with 20 ng Tbx1 MO (76%,  $n = 25$ ) (Fig. 4). No delays in migration were observed when the subphenotypic MO doses were supplemented with 20 ng of control MO in order to compensate for potential non-specific effects of higher morpholino concentrations ( $n = 25$  for each set-up). All together, these data indicate that ARVCF and Tbx1 act cooperatively in the generation of structures derived from CNCC.

### DISCUSSION

We provide evidence that the reduction of the armadillo protein ARVCF plays a role in the molecular etiology of 22q11.2DS. First, we found that ARVCF transcripts in *Xenopus* are present in regions or tissues affected in 22q11.2DS, e.g., the pharyngeal arches and the heart. Second, depletion of ARVCF generates defects in the craniofacial cartilage structures and in the aortic arches. These malformations are also observed in 22q11.2DS patients. Third, we found that ARVCF cooperates with Tbx1, a transcription factor previously associated with the etiology of 22q11.2DS. Furthermore, we demonstrate that the malformation of the cartilage in ARVCF-depleted embryos is associated with delayed migration of neural crest cells, similar to what has recently been described for Tbx1 depletion (Tazumi et al., 2010).

Mice with a single *Arvcf* knock-out have not been reported. However, mice with a heterozygous 550-kb deletion of the 22q11 region encompassing 16 genes, including *Arvcf* but not *Tbx1*, do not develop any cardiovascular phenotypic alteration (Puech et al., 2000). This argues that the absence of ARVCF or any of these 16 genes, individually or in combination, is not responsible for the cardiovascular abnormalities associated with 22q11.2DS. Although this argues

**Fig. 4.** Effects of ARVCF or Tbx1 depletion on neural crest cell specification and migration. Embryos were injected unilaterally with 50 ng ARVCF MO, Tbx1 MO, or control MO, or with a combination of the two MOs at a subphenotypic dose (20 ng). RNA encoding  $\beta$ -galactosidase was coinjected as a tracer. Embryos were fixed at stage 20, 27, and 32 and processed for in situ hybridization with a probe directed against *Twist*. Injection of ARVCF MO or Tbx1 MO does not interfere with the induction of neural crest cells (NCC) and the mandibular (m), hyoid (h), and branchial (br) streams can be easily discerned at stage 20. The injected side is marked by an asterisk. However, at stages 20 and 27, the migration of *Twist*-positive NCCs is delayed in the side injected with ARVCF MO or Tbx1 MO compared to the non-injected side. The delay is even greater in embryos injected with a combination of ARVCF and Tbx1 MO at a sub-phenotypic dose (20 ng). At stage 32, *Twist* patterns are largely identical in the injected and non-injected sites, indicating that all CNCCs have ultimately reached their final destination.

**Fig. 5.** Cooperative effect of the depletion of ARVCF and Tbx1. **A:** Fifty nanograms of control MO (a–c) or combined subphenotypic doses of ARVCF MO and Tbx1 MO (d–f) were injected at the one-cell stage. Tadpoles are shown alive at stage 48 (a,d), fixed and stained with Alcian Blue to reveal the cartilage structures (b,e), or stained with the von Willebrand factor antibody to reveal the aortic arches (c,f). Simultaneous depletion of ARVCF and Tbx1 results in malformation of cartilage, as seen in a living embryo (d) and after Alcian Blue staining (e), compared with the control embryos (a, b). Depletion of both ARVCF and Tbx1 also results in defects in aortic arch formation and frequent absence of arch 5 (f). **B:** The cooperative effect was also manifested in the width of the head. Embryos injected with a combination of subphenotypic doses of ARVCF and Tbx1 MO had significantly narrower heads than tadpoles injected with either control, Tbx1, or ARVCF MO ( $P = 0.0017$ ).



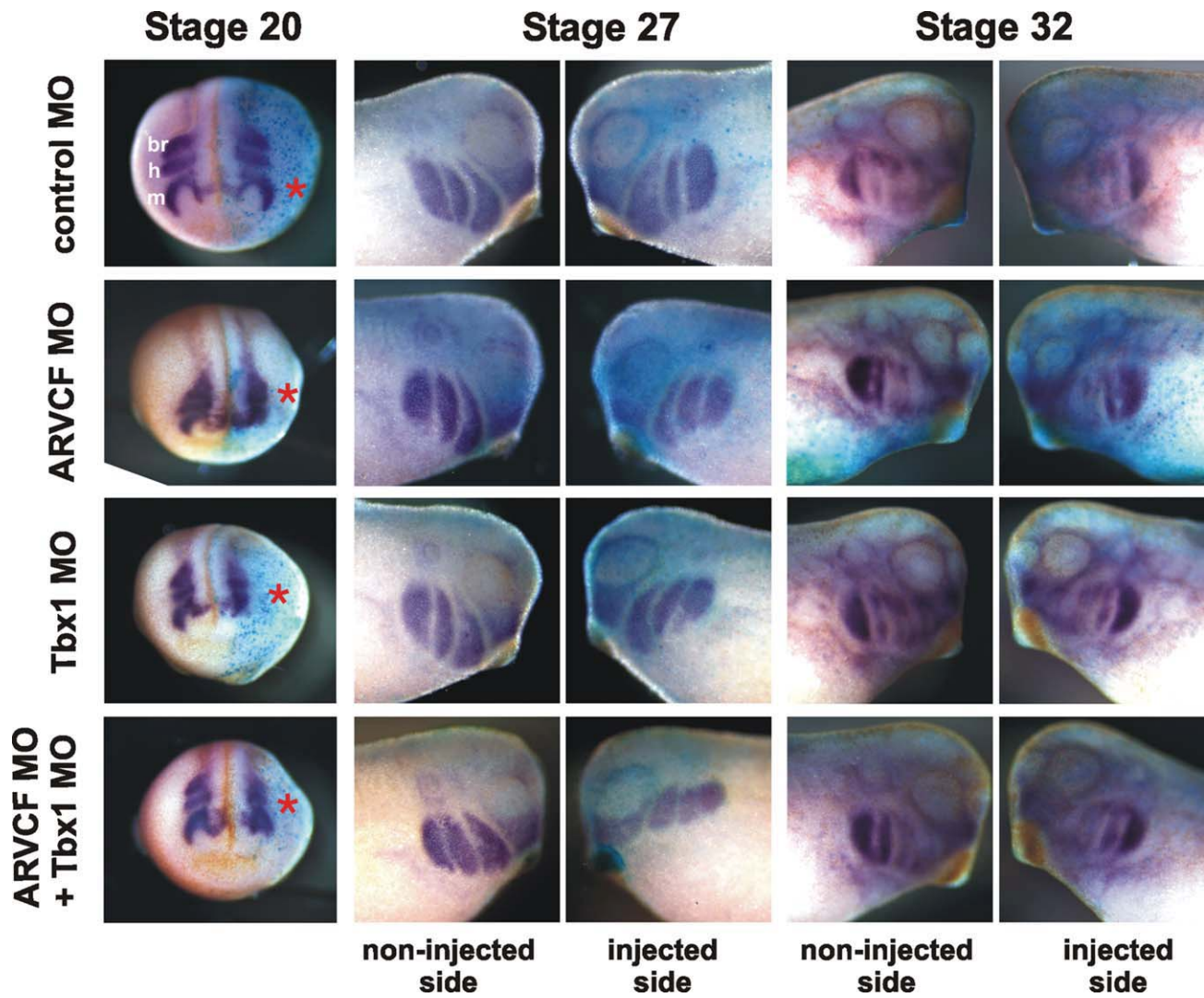


Fig. 4.

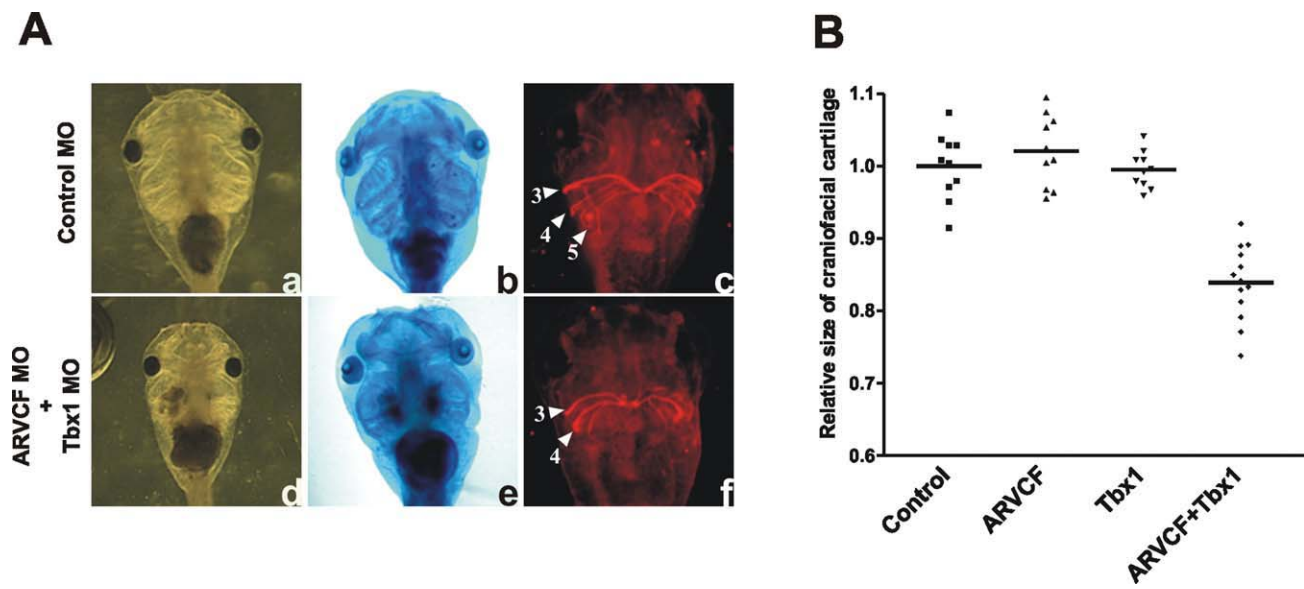


Fig. 5.

against a dominant or central role for *ARVCF* in the development of the physical abnormalities associated with 22q11.2DS and supports the well-documented central role of *Tbx1*, it does not fully exclude the possibility that *ARVCF* defects cooperate with defects in one or more genes that are consistently deleted in the syndrome.

In *Xenopus*, injection of a dominant-negative *Tbx1* mutant leads to malformations in the head cartilage, hypoplasia of the pharyngeal apparatus, impaired looping of the heart, and pericardial edema (Ataliotis et al., 2005) as well as disruption of the interhyoid muscle (Smith et al., 2005). Morpholino-mediated depletion induces a delay in CNCC migration and impaired development of the cranial cartilage (Tazumi et al., 2010). Interestingly, defects in cardiac neural crest cell migration have been observed in the context of *Tbx1* haploinsufficiency in the mouse (Calmont et al., 2009).

In our study, we confirm, using a different morpholino, that depletion of *Tbx1* in *Xenopus* leads to defects in the head cartilage but found that the aortic arches are also affected. This is further in line with the previous studies in mice and zebrafish that showed the key role of *Tbx1* in the development of pharyngeal arch derivatives (Jerome and Papaioannou, 2001; Lindsay, 2001; Merscher et al., 2001; Piotrowski et al., 2003). Our data show now that correct formation of the structures associated with the pharyngeal arches requires cooperation of *ARVCF* with *Tbx1*. We demonstrate this by simultaneously depleting *ARVCF* and *Tbx1* using concentrations of MOs that are ineffective when used individually. Interestingly, the effects of *ARVCF* depletion on the migration of CNCC and on the formation of the cranial cartilage structures were also found in an independent study (Cho et al., 2011). However, in their study, a moderate effect of *ARVCF* depletion on neural crest specification was described. We only detected minor or no effects of *ARVCF* depletion on expression of the neural crest markers *Twist* or *Slug*. We suspect that these effects may be dependent on the efficiency of *ARVCF* depletion.

In summary, we demonstrate that *ARVCF* and *Tbx1* are both required

for the correct formation of the craniofacial cartilage and the aortic arches of *Xenopus*, both of which are affected in 22q11.2DS. Furthermore, we found that depletion of *ARVCF* and/or *Tbx1* delays the migration of CNCC, which is possibly responsible for the observed malformation of the head cartilage and the aortic arches. We conclude that *ARVCF* and *Tbx1* are important during the development of *X. laevis* and that this organism is a suitable model for studying processes associated with 22q11.2DS.

## EXPERIMENTAL PROCEDURES

### Whole-Mount In Situ Hybridization

To make sense and antisense probes directed against *xARVCF*, an 807-bp fragment (bp 1611–2418) from pCS2+*ARVCF* (Paulson et al., 2000) was cloned in pBluescript. The resultant plasmid was linearized with *Bam*HI and *Sma*I. The plasmids containing the *Twist* and the *Slug* probe were linearized with *Eco*RI and *Nde*I, respectively. Digoxigenin was incorporated in the probes according to the manufacturer's instructions (Roche, Indianapolis, IN). In situ hybridization was performed as described (Ciesiolka et al., 2004).

### Morpholino and RNA Injections

To deplete *ARVCF*, the *ARVCF* MOII was used as described (Fang et al., 2004). The morpholino directed against *Tbx1* was designed by Gene Tools (Philomath, OR) and has the following sequence: 5'CCGAGATCATCC CAGGAATAGACAG3'. The control MO is a standard morpholino provided by Gene Tools. The morpholinos and RNAs were microinjected in *X. laevis* embryos as described (Ciesiolka et al., 2004). For tracing experiments, RNA encoding  $\beta$ -galactosidase or a lysamine-labeled control MO was coinjected with the morpholinos targeting *ARVCF* or *Tbx1*. To assess the efficiency of the *Tbx1* morpholino, a HA-tag was added to the C-terminus of *xTbx1* in the plasmid  $\beta$ UT2-*xTbx1a* (kindly provided by Peter Scambler) using the QuickChange site-directed

mutagenesis kit (Stratagene, La Jolla, CA). The tagged cDNA was subcloned in pCS2+, linearized, and used for RNA synthesis using the mMES-SAGE mMACHINE® SP6 Kit (Ambion, Austin, TX). For rescue experiments, RNAs were injected that lack the sequence targeted by the morpholinos.

### Immunostaining, Alcian Blue Staining, and Head Measurements

Embryos were fixed in Dents fixative (20% DMSO, 80% methanol) overnight at  $-20^{\circ}\text{C}$ . Embryos were rehydrated stepwise, washed in PBS, preincubated in TBS with 2% BSA, and incubated overnight at  $4^{\circ}\text{C}$  with primary antibody (von Willebrandt Factor, 1:100, Dako, Haverlee, Belgium). Next, embryos were washed in PBS containing 0.1% Triton X100, blocked with 2% BSA in PBS, and incubated overnight with secondary antibody (anti-rabbit Alexa 594, 1:500, Molecular Probes, Eugene, OR; Invitrogen, Carlsbad, CA). Finally, they were washed with PBS/0.1% Tween 20. Images were taken with a Leica MZFLIII fluorescence stereomicroscope. Alcian blue staining was performed as described (Pasqualetti et al., 2000). The width of the head was plotted by measuring the widest point of the ceratobranchial and Meckel's cartilage structures as indicated in Figure 2Ba and adding the two values.

### Micro CT-Scanning

Embryos were injected at the four-cell stage with *ARVCF*, *Tbx1*, or Control MO in one dorsal blastomere and left to develop until stage 48, when they were fixed in 4% paraformaldehyde in PBS and further stained with 2.5% phosphotungstic acid. Next, the tadpoles were dehydrated stepwise until ethanol 70%. Finally, they were scanned by micro-CT. The images were imported into Amira 5.3.3 order to generate a 3D reconstruction of each tadpole.

### ACKNOWLEDGMENTS

We thank E. Bellefroid, G. Roël, and O. Destree for their generous gift of the

Slug and Twist plasmid and Peter Scambler for the Tbx1 construct. We thank Denis Van Loo from the Centre for X-ray Tomography (UGCT) for generating the CT images. We are indebted to G. Van Imschoot for help throughout the project and to A. Breddan for editing the manuscript.

## REFERENCES

- Ataliotis P, Ivins S, Mohun TJ, Scambler PJ. 2005. XTbx1 is a transcriptional activator involved in head and pharyngeal arch development in *Xenopus laevis*. *Dev Dyn* 232:979–991.
- Baldini A. 2005. Dissecting contiguous gene defects: TBX1. *Curr Opin Genet Dev* 15:279–284.
- Calmont A, Ivins S, Van Bueren KL, Papanageli I, Kyriakopoulou V, Andrews WD, Martin JF, Moon AM, Illingworth EA, Basson MA, Scambler PJ. 2009. Tbx1 controls cardiac neural crest cell migration during arch artery development by regulating Gbx2 expression in the pharyngeal ectoderm. *Development* 136:3173–3183.
- Cho K, Lee M, Gu D, Munoz W, Ji H, Kloc M, McCrea P. 2011. Kazrin, and its binding partners ARVCF- and delta-catenin, are required for *Xenopus* craniofacial development. *Dev Dyn* 240:2601–2612.
- Ciesiolka M, Delvaeye M, Van Imschoot G, Verschuere V, McCrea P, Van Roy F, Vleminckx K. 2004. p120 catenin is required for morphogenetic movements involved in the formation of the eyes and the craniofacial skeleton in *Xenopus*. *J Cell Sci* 117:4325–4339.
- Davis MA, Ireton RC, Reynolds AB. 2003. A core function for p120-catenin in cadherin turnover. *J Cell Biol* 163:525–534.
- Fang X, Ji H, Kim SW, Park JJ, Vaught TG, Anastasiadis PZ, Ciesiolka M, McCrea PD. 2004. Vertebrate development requires ARVCF and p120 catenins and their interplay with RhoA and Rac. *J Cell Biol* 165:87–98.
- Hatzfeld M. 2005. The p120 family of cell adhesion molecules. *Eur J Cell Biol* 84:205–214.
- Jerome LA, Papaioannou VE. 2001. DiGeorge syndrome phenotype in mice mutant for the T-box gene, Tbx1. *Nat Genet* 27:286–291.
- Levine AJ, Munoz-Sanjuan I, Bell E, North AJ, Brivanlou AH. 2003. Fluorescent labeling of endothelial cells allows in vivo, continuous characterization of the vascular development of *Xenopus laevis*. *Dev Biol* 254:50–67.
- Lindsay EA. 2001. Chromosomal microdeletions: dissecting del22q11 syndrome. *Nat Rev Genet* 2:858–868.
- Merscher S, Funke B, Epstein JA, Heyer J, Puech A, Lu MM, Xavier RJ, Demay MB, Russell RG, Factor S, Tokooya K, Jore BS, Lopez M, Pandita RK, Lia M, Carrion D, Xu H, Schorle H, Kobler JB, Scambler P, Wynshaw-Boris A, Skoultschi AI, Morrow BE, Kucherlapati R. 2001. TBX1 is responsible for cardiovascular defects in velo-cardio-facial/DiGeorge syndrome. *Cell* 104:619–629.
- Moody SA. 1987. Fates of the blastomeres of the 16-cell stage *Xenopus* embryo. *Dev Biol* 119:560–578.
- Pasqualetti M, Ori M, Nardi I, Rijli FM. 2000. Ectopic Hoxa2 induction after neural crest migration results in homeosis of jaw elements in *Xenopus*. *Development* 127:5367–5378.
- Paulson AF, Mooney E, Fang X, Ji H, McCrea PD. 2000. Xarvcf, *Xenopus* member of the p120 catenin subfamily associating with cadherin juxtamembrane region. *J Biol Chem* 275:30124–30131.
- Paylor R, Glaser B, Mupo A, Ataliotis P, Spencer C, Sobotka A, Sparks C, Choi CH, Oghalai J, Curran S, Murphy KC, Monks S, Williams N, O'Donovan MC, Owen MJ, Scambler PJ, Lindsay E. 2006. Tbx1 haploinsufficiency is linked to behavioral disorders in mice and humans: implications for 22q11 deletion syndrome. *Proc Natl Acad Sci USA* 103:7729–7734.
- Piotrowski T, Ahn DG, Schilling TF, Nair S, Ruvinsky I, Geisler R, Rauch GJ, Haffter P, Zon LI, Zhou Y, Foote H, Dawid IB, Ho RK. 2003. The zebrafish van gogh mutation disrupts tbx1, which is involved in the DiGeorge deletion syndrome in humans. *Development* 130:5043–5052.
- Puech A, Saint-Jore B, Merscher S, Russell RG, Cherif D, Sirotkin H, Xu H, Factor S, Kucherlapati R, Skoultschi AI. 2000. Normal cardiovascular development in mice deficient for 16 genes in 550 kb of the velocardiofacial/DiGeorge syndrome region. *Proc Natl Acad Sci USA* 97:10090–10095.
- Rauch A, Devriendt K, Koch A, Rauch R, Gewillig M, Kraus C, Weyand M, Singer H, Reis A, Hofbeck M. 2004. Assessment of association between variants and haplotypes of the remaining TBX1 gene and manifestations of congenital heart defects in 22q11.2 deletion patients. *J Med Genet* 41:e40.
- Smith SJ, Ataliotis P, Kotecha S, Towers N, Sparrow DB, Mohun TJ. 2005. The MLC1v gene provides a transgenic marker of myocardium formation within developing chambers of the *Xenopus* heart. *Dev Dyn* 232:1003–1012.
- Stoller JZ, Epstein JA. 2005. Identification of a novel nuclear localization signal in Tbx1 that is deleted in DiGeorge syndrome patients harboring the 1223delC mutation. *Hum Mol Genet* 14:885–892.
- Tazumi S, Yabe S, Uchiyama H. 2010. Paraxial T-box genes, Tbx6 and Tbx1, are required for cranial chondrogenesis and myogenesis. *Dev Biol* 346:170–180.
- Wilson V, Conlon FL. 2002. The T-box family. *Genome Biol* 3: Reviews3008.
- Yagi H, Furutani Y, Hamada H, Sasaki T, Asakawa S, Minoshima S, Ichida F, Joo K, Kimura M, Imamura S, Kamatani N, Momma K, Takao A, Nakazawa M, Shimizu N, Matsuoka R. 2003. Role of TBX1 in human del22q11.2 syndrome. *Lancet* 362:1366–1373.
- Yamagishi H, Srivastava D. 2003. Unraveling the genetic and developmental mysteries of 22q11 deletion syndrome. *Trends Mol Med* 9:383–389.